KSCE Journal of Civil Engineering (2018) 22(10):3995-4010
DOI 10.1007/s12205-018-1518-0

Structural Engineering
pISSN 1226-7988, eISSN 1976-3808
www.springer.com/12205

Experimental Investigation on Vulnerability of Precast RC Beam-column Joints to Progressive Collapse

Tarek H. Almusallam*, Hussein M. Elsanadedy, Yousef A. Al-Salloum***, Nadeem A. Siddiqui****, and Rizwan A. Iqbal*****

Received October 2, 2017/Revised 1st: December 12, 2017, 2nd: January 8, 2018/Accepted February 1, 2018/Published Online July 23, 2018

Abstract

The multi-story buildings are susceptible to progressive collapse in the event of the removal of one or more columns due to the exposure to blast loads. The lack of structural continuity in precast concrete buildings makes these buildings more vulnerable to progressive collapse as compared to the regular cast-in-situ concrete buildings. This study presents experiments involving two types of detailing of precast beam-column joints using half-scale test specimens when the middle column is suddenly removed. The test specimens represent the most prevalent precast beam-column joints. One conventional cast-in-situ test specimen, having continuous top and bottom beam rebars, was used for comparison. The progressive collapse scenario was simulated by removing the central column support and applying a sudden vertical load on this column at a rate of 100 mm/s until failure. Test results helped in developing better understanding about the progressive collapse potential in the existing precast buildings. This study highlights the need for the rehabilitation of beam-column connections in existing precast buildings and necessitates the need for innovative beam-column connections for improving the progressive collapse resistance.

Keywords: *progressive collapse, precast, beam-column connection, blast loads, testing*

1. Introduction

The precast Reinforced Concrete (RC) structures are preferred mainly because of the ease of their constructability. In the last few decades, precast RC structures have gained popularity in Saudi Arabia. The structural elements are produced in factories in a controlled environment and transported to the site where the individual elements are assembled and connected. Examples of typical precast buildings within Saudi Arabia are given in Fig. 1.

Buildings are extremely vulnerable to progressive collapses due to the loss of one or more axial load-carrying members (e.g. columns). Progressive collapse is generally defined as propagation of an initial local failure from one structural element to another and eventually leading to a complete collapse or the collapse of a major portion of the structure. Progressive collapse of a structure usually causes great loss of life and property. It is, therefore, important to study the potential of precast concrete structures for progressive collapse to avoid catastrophic events. As the precast RC buildings greatly lack in the structural continuity and redundancy in the load paths (i.e. ability to bridge over vertical load-bearing elements that are suddenly removed in an extreme event such as blast loads), these are more vulnerable to progressive collapse as compared to the conventional cast-in-situ RC structures.

One of the approaches to assess progressive collapse is to study the effects of sudden removal of vertical load-carrying members (such as a column) on the rest of the structure, and to check if any other alternate load paths do exist thereby arresting the damage initiation from propagating from one element to another. Research on progressive collapse of structures was conducted by: Pourasil *et al.* (2017), Elkoly and El-Ariss (2014), Peakau and Cui (2006), Allen and Schriever (1972), Almusallam *et al.* (2010), Elsanadedy *et al.* (2014), Choi and Chang (2009), Al-Salloum *et al.* (2015), Dat *et al.* (2015), Bao *et al.* (2008), and others. Sasani *et al.* (2007) assessed the progressive collapse risk of an actual 10-story RC structure due to sudden removal of an exterior column because of blast threat scenario. Yu and Tan (2013) studied the influence of seismic detailing on structural behavior under a column-loss scenario. The experimental program involved testing of half-scale test specimens. The seismic and non-seismic details were considered to assess the influence of

*Professor, Dept. of Civil Engineering, King Saud University, Riyadh 11421, Saudi Arabia (E-mail: musallam@ksu.edu.sa)
**Associate Professor, Dept. of Civil Engineering, King Saud University, Riyadh 11421, Saudi Arabia; on Leave from Helwan University, Cairo, Egypt (Corresponding Author, E-mail: elsanadedy@yahoo.com)
***Professor, Chair of Research and Studies in Strengthening and Rehabilitation of Structures, Dept. of Civil Engineering, King Saud University, Riyadh 11421, Saudi Arabia (E-mail: ysalloum@ksu.edu.sa)
****Professor, Dept. of Civil Engineering, King Saud University, Riyadh 11421, Saudi Arabia (E-mail: nadeem@ksu.edu.sa)
*****Research Engineer, Dept. of Civil Engineering, King Saud University, Riyadh 11421, Saudi Arabia (E-mail: rizo59s@gmail.com)

Al-Rashed Mall, Al-Khobar, K.S.A.

Precast beam-column connection Type-A

(a)

King Saud University Girls Campus, Riyadh, K.S.A

Precast beam-column connection Type-B

(b)

Fig. 1. Examples of Typical Beam-column Connections in Precast Buildings in Saudi Arabia: (a) Precast Type-A Beam-column Connection, (b) Precast Type-B Beam-column Connection

rebar detailing on structural performance. Different structural mechanisms, namely, flexure, compressive arch action and catenary formation were observed.

The behavior of precast RC beam-column assemblies under sudden column-loss scenario depends mainly on the continuity at the precast beam-column joints. Even though continuity of different designs of precast RC beam-column connections has not been intensively studied in the literature under abrupt column-loss scenarios, it has been thoroughly investigated under quasi-static lateral cyclic loading simulating seismic actions (Choi *et al.*, 2013; Ertas *et al.,* 2006; Joshi *et al*., 2005; Panedpojaman *et al.*, 2016; Parastesh *et al*., 2014; Shariatmadar and Beydokhti, 2011; Vidjeapriya and Jaya, 2012; Vidjeapriya and Jaya, 2013; Wahjudi *et al.*, 2014). In all of these studies, different designs for interior (or exterior) precast RC beam-column connection assemblies were studied under simulated seismic loading. The behavior of precast connections was evaluated in terms of load-displacement characteristics and the performance was then compared with their monolithic counterparts.

Kang and Tan (2015) studied experimentally the behavior of precast RC beam-column assemblies under column-removal scenario. The beams and columns were joined together by cast-in-situ concrete topping above the two adjoining beams and the connection. The top longitudinal rebars passed through the joint continuously. The middle joint detailing involved, 90° bend and lap-splice of bottom rebars. The specimens were tested to failure under quasi-static loads. It was concluded that the continuity of top reinforcement along with the cast-in-situ concrete topping led to the development of Compressive Arch Action (CAA) and catenary action. However, the CAA and catenary action capacities were overestimated due to the rigid boundary conditions adopted in experiments. In another study, Kang *et al.* (2015) studied the progressive collapse behavior of precast RC beam-column sub-assemblages produced using Engineered Cementitious Composites (ECC) in cast-in-situ structural toppings and joints under column-loss scenarios. Results of the experiments indicated that the development of CAA and catenary action was sequential with increasing vertical joint displacement. Unlike conventional cast-in-situ RC, structural ECC topping showed multi-cracking behavior with distributed cracks.

In a recent study, Elsanadedy *et al.* (2017) developed a nonlinear Finite Element (FE) model using LS-DYNA software (LSTC, 2007) to predict the performance of precast non-prestressed RC beam-column assemblies under sudden column-removal scenario. The FE model considered the nonlinear behavior of concrete and steel, strain rate effect on material properties and contact between surfaces at the joints. The FE model was calibrated against some of the test results of the current study. The validated FE modeling was further extended to investigate the progressive collapse potential of different designs of precast RC beam-

column connections. Because of the FE study, new joint efficiency parameters were developed.

Numerous studies have been carried out on progressive collapse performance of framed monolithic structures under column-loss scenarios. Literature review also suggests many studies on the different types of beam-column connections in precast structures. However, there are very few studies, which focus on the progressive collapse of precast structures under column-removal scenario. Precast structures are widely used in residential and commercial buildings throughout the world. As a result, any collapse of precast structures would result in huge losses of life and property. For this reason, it is necessary to conduct research on the progressive collapse performance of precast structures and suggest methodologies to improve their behavior under such scenarios.

The goal of this research was to study experimentally the progressive collapse potential of existing types of precast RC beam-column connections under abrupt column-removal scenarios based on the scaling of an existing prototype building. The novelty of this research is that this experimental work has not been published in the literature including our earlier work (Elsanadedy *et al.*, 2017). This paper presents experiments involving two types of half-scale precast RC specimens tested under middle column-loss scenario. The test specimens represented

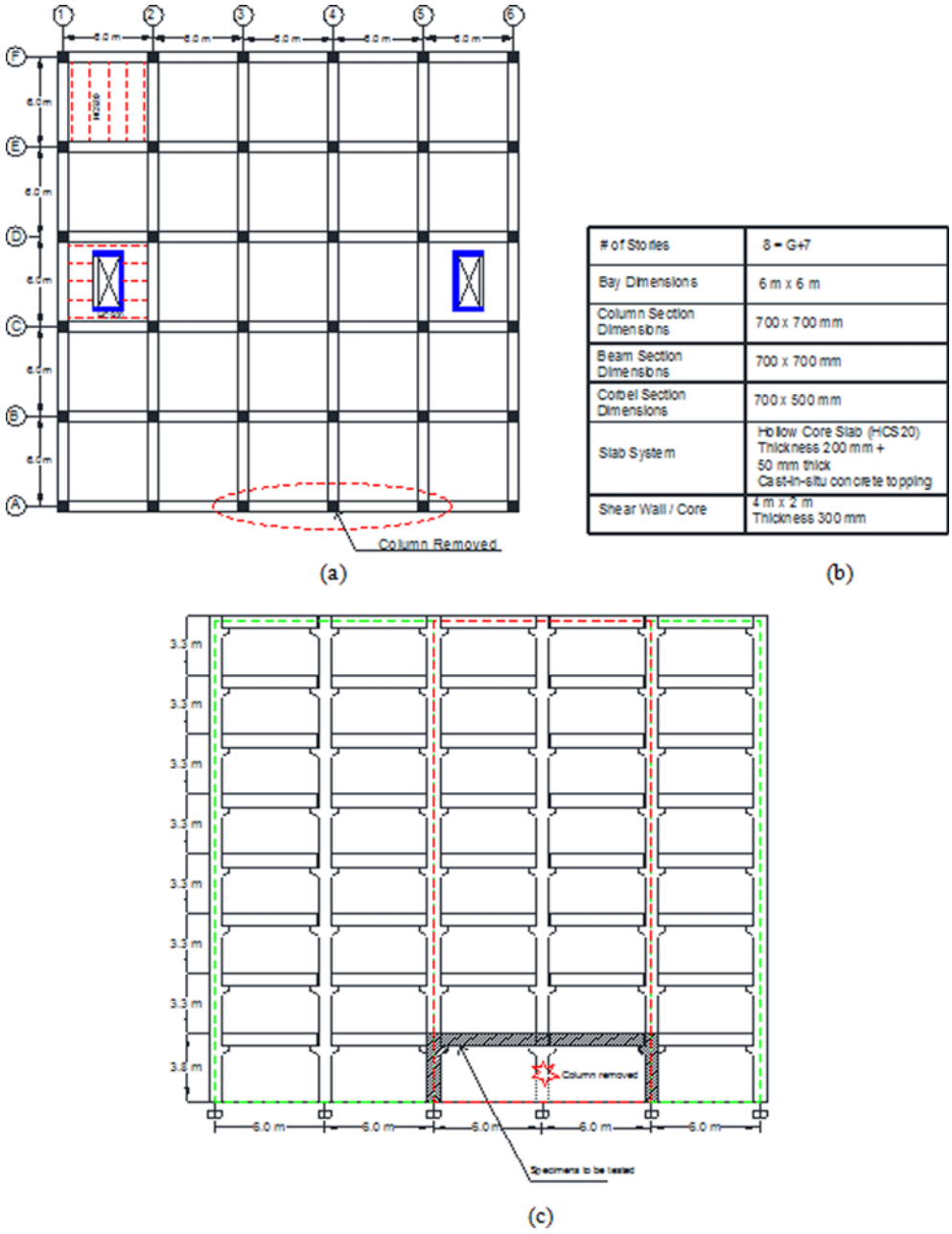

Fig. 2. Location of the Prototype of Test Specimens: (a) Plan View of Prototype Building, (b) Structural Details, (c) Elevation View of the Prototype Building

Table 1. Geometric Properties of Prototype Frames and Test Specimens

Type	Beam net span (mm)	Beam size (mm)		Column size (mm)	Corbel size (mm)	Type of connection
		Depth	Width			
Prototype	5240	700	700	700 × 700	700 × 500	Precast
Specimen PC-A	2620	350	350	350 × 350	350 × 250	Precast with grouting of corbel rebar
Specimen PC-B	2620	350	350	350 × 350	350 × 250	Precast with grouting of corbel rebar and welding of steel plate with angles
Specimen MC-SMF	2650	350	350	350 × 350	—	Monolithic

the most prevalent types of existing precast RC beam-column joints in Saudi Arabia. One cast-in-situ test specimen having continuity of top and bottom beam rebars was used for the sake of comparison. The test specimens were tested under middle column-loss scenario with the middle column being exposed to high rate dynamic loading at a displacement rate of 100 mm/s in order to simulate the progressive collapse in real structures. Performance of precast test specimens was investigated and compared with the cast-in-situ test specimen.

2. Experimental Program

The experimental program comprised of testing three half-scale specimens, which were designed and tested under the column-loss scenario. Two of the specimens were precast with beams and columns cast individually and subsequently assembled on test bed for simulating the field conditions. The other test specimen was monolithic. All specimens consisted of two-bay beams and three columns. Special test rig was used to support the specimens and displacement controlled loading was applied to the middle column until the specimens failed completely.

2.1 Design of Specimens

It should be noted that for a commercial building, the perimeter bays are most susceptible to any kinds of attacks owing to the ease of accessibility. For this reason, the selected two-bay frame prototype specimens were assumed to be a part of a middle-bay perimeter frame of a commercial precast building located at a busy intersection of Riyadh (Fig. 2). The selected 8-story building had a ground floor with a height of 3.8 m and the typical floors had a height of 3.3 m. The spans in both the orthogonal directions were 6.0 m each. The live load used for the design was 4 kN/m^2 and the total superimposed dead load was 5 kN/m^2. A uniform line dead load of 16.3 kN/m was also used which simulated the exterior non-structural façade components on the perimeter frames (230 mm thick precast exterior panels). The building is located in the city of Riyadh, which is considered a non-seismic zone. Two U-shape RC cores were present as shown in the plan view of the building (Fig. 2(a)) to resist lateral loading on the structure due to wind loads. The building was designed in conformance with the ACI 318-08 code (ACI 2008). The test specimens were designed to be half-scale of the prototype perimeter frame. Fig. 2(c) shows the elevation view of the prototype building, in which the directly affected part (as a result of removal of the column) is shown using red-dotted lines. As shown in the figure, this is the part directly above the removed column. On the same figure, the indirectly affected part due to the re-distribution of loads, is represented by green dotted lines. As a result of column removal, a doubling of span will be induced for the region shaded in Fig. 2(c) and also amplification of vertical loads will be noticed for this region making it the most critical element in the frame.

The test matrix used in this study comprised of three half-scale specimens. Two specimens (PC-A and PC-B) were precast non-prestressed and the third specimen MC-SMF was monolithic with continuous bottom and top beam reinforcement through the connection region. The geometric dimensions for both the prototype and the specimens are presented in Table 1. The test matrix was designed to study the behavior of existing precast beam-column joints under column-loss scenario and compare their behavior to that of monolithic specimen under collapse loading scenario. Precast specimens PC-A and PC-B were prepared with beam and column members cast individually and then assembled on test bed for simulating the field conditions. The two specimens differed from each other in terms of beam-column connections. The concrete dimensions and reinforcement details for PC-A specimen are shown in Fig. 3. For both columns and beams, section sizes of 350 × 350 mm were used and the corbels had section dimensions of 350 × 250 mm. As shown in Fig. 3, the height of the column to the bottom of the beam was 1050 mm and the columns were made to rest on a steel I-shaped stub of height 500 mm making the total height of test specimen as 1550 mm. The steel stubs were then connected to the steel rails made of I-sections that were anchored to the strong test floor. It should be noted that the steel I-shaped stubs, connected to the lower part of the RC columns, were designed so that their flexural stiffness is approximately the same as that for the RC columns. Longitudinal reinforcement of beams comprised of 4ϕ16 mm rebars on both tension and compression sides and 2 legged ϕ8 mm rebars used as stirrups at 100 mm center-to-center spacing. The longitudinal reinforcement for columns comprised of 8ϕ16 mm rebars, and ϕ8 mm ties were provided as transverse reinforcement at variable spacing, as shown in Fig. 3. The center-to-center distance between columns was kept as 3 m. The PC-A beam-column connection is composed of a corbel rebar grouted with the beam on both the beam ends. The concrete dimensions and reinforcement details for PC-B specimen are depicted in Fig. 4. The precast specimen PC-B differs from PC-A specimen in

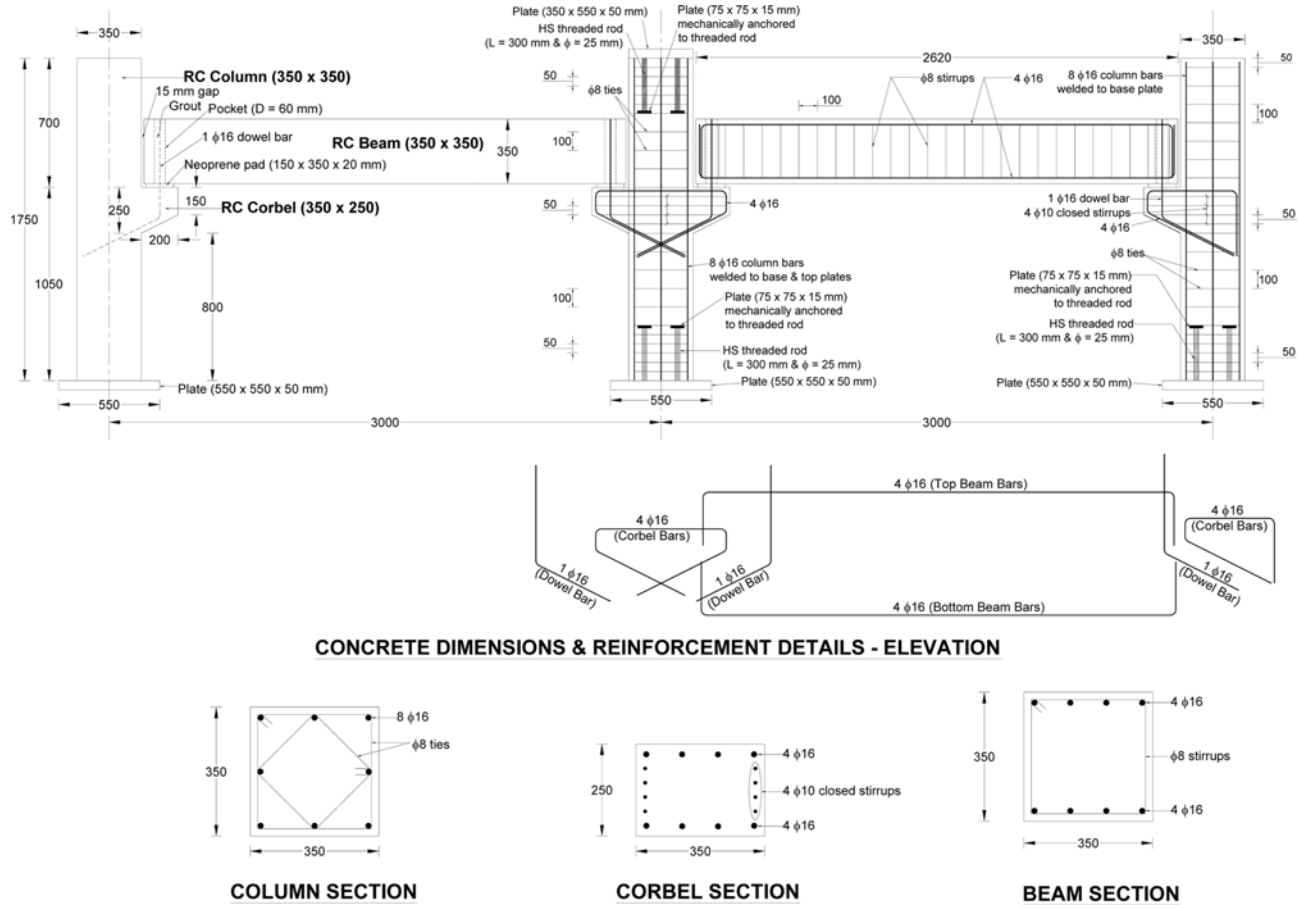

Fig. 3. Details of Precast Specimen PC-A (Note: All dimensions are in mm)

terms of beam-column connection. Two pockets of diameter 60 mm were left out at both the beam ends for grouting purposes. The center-to-center distance between the columns was kept the same as 3 m. One other specimen monolithically cast (MC-SMF) was also used in the experimental program. This specimen was detailed with continuous top and bottom beam reinforcement. Concrete dimensions and reinforcement details of specimen MC-SMF are given in Fig. 5.

2.2 Preparation and Assembly of Specimens

Before casting of specimens, the base and top steel plates for column ends were fabricated in the workshop. The 40 mm thick steel base plate for the two end columns was embedded in the column concrete using 5-25 mm diameter high strength threaded rods which were mechanically anchored as well as groove welded to the base plate. A 75 × 75 × 15 mm plate was mechanically anchored to the top of the high strength threaded rods. The 8-16 mm diameter longitudinal rebars of the column were then welded to the base plate. For the middle column which would be attached to the actuator, a 40 mm top plate was embedded at the top of column. The top plate was embedded similar to the base plate. Similarly, for the case of middle column, the rebars were welded to the top plate. This was done in order to avoid any local failure of column ends as a result of load application.

Once the steel work was completed, fabrication of wooden formwork was started. For the two precast specimens, the beams and columns were cast individually and were later assembled at the test rig. Since these specimens are precast, care was taken to make sure the dimensions of the formwork were accurate. However, for the monolithic specimen, the complete two-bay frame wooden formwork was prepared and was filled with concrete. The specimen was then transported to the test rig as one single monolithic frame comprising of two beams and three columns. Fig. 6 summarizes the steps involved in the preparation of the three specimens of this study; whereas Fig. 7 shows the steps involved in the assembly of the precast specimens on the test rig. The assembly of precast specimens was carried out as in the field. Fig. 7(a) shows the steel rails on which the specimen rested. The steel rails made of I-sections, were anchored to the strong test floor. As seen in the figure, special column supports were fabricated and connected to the rails to support the columns. All three columns were first erected on the column supports. The neoprene pads were then placed on corbel locations and the beam, which was carried by overhead crane, was then brought and slowly lowered to rest on corbels. It was made sure that the single corbel rebar went through the beam pockets at both the ends, which were grouted later. For the case of PC-A specimen, the beam had hollow circular pockets of

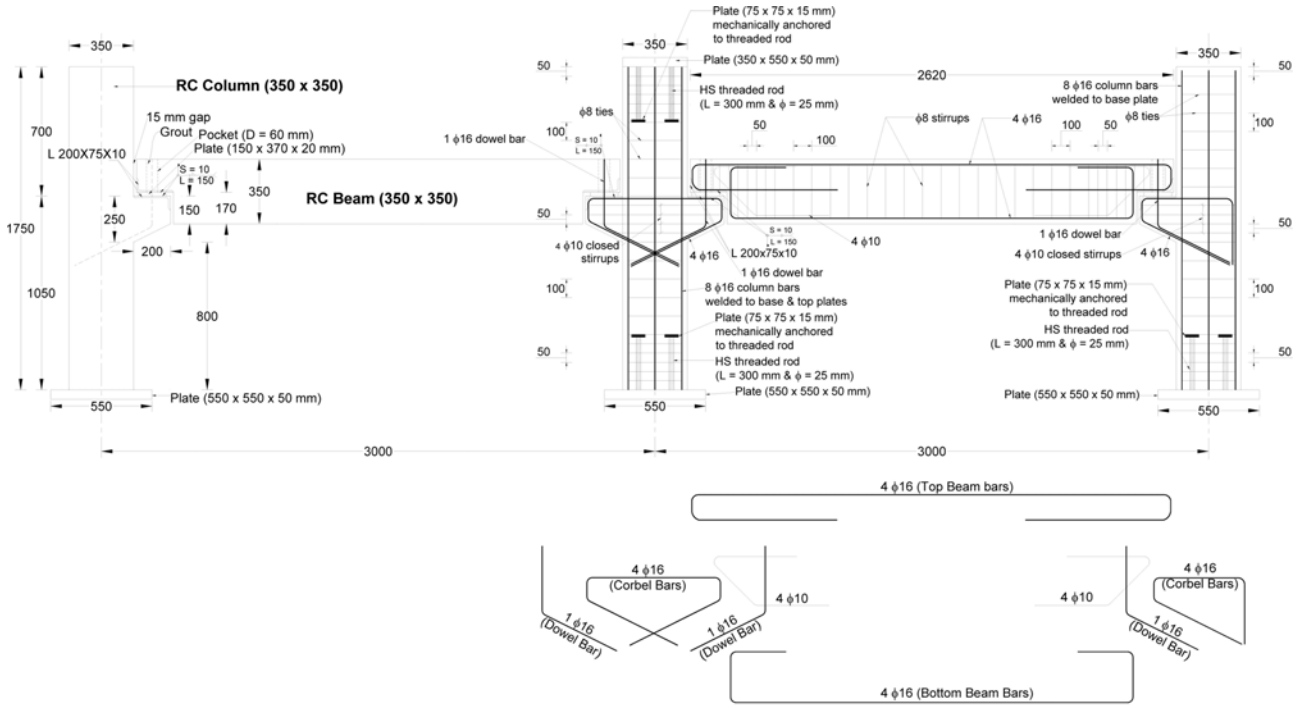

Fig. 4. Details of Precast Specimen PC-B (Note: All dimensions are in mm)

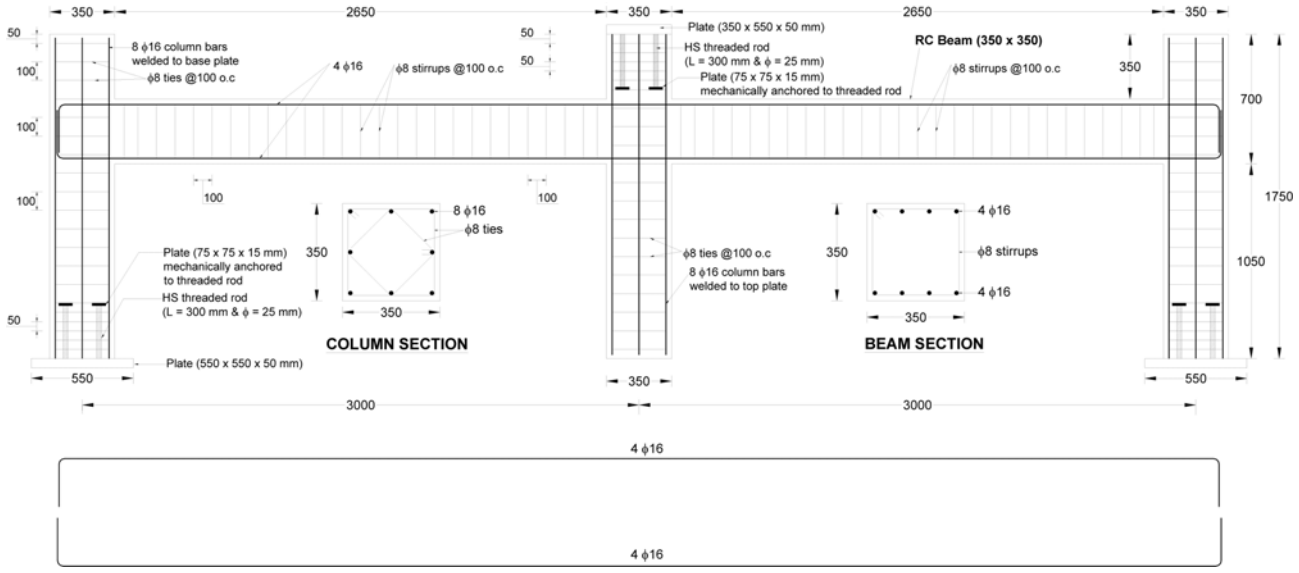

Fig. 5. Details of Monolithic Specimen MC-SMF (Note: All dimensions are in mm)

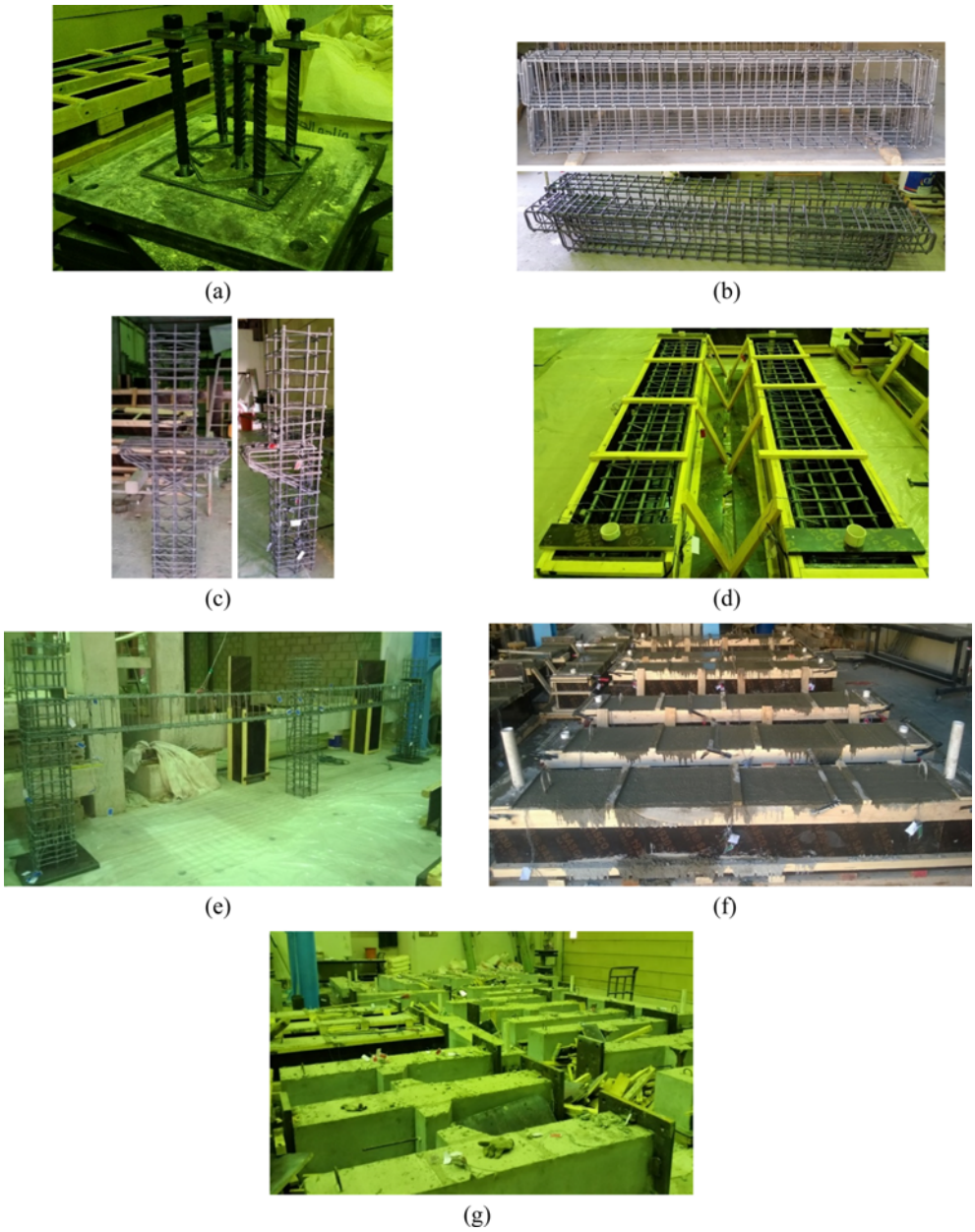

Fig. 6. Preparation of Test Specimens: (a) Base Plate with Anchor Rods, (b) Reinforcement Cage for Beams of Precast Specimens, (c) Reinforcement Cage for Columns of Precast Specimens, (d) Reinforcement Cages Placed in Wooden Formwork, (e) Reinforcement Cage for Monolithic Specimen MC-SMF, (f) Casting of Precast Elements, (g) Individual Precast Elements after Demolding

diameter 60 mm for the corbel rebar to pass through. Before grouting, the beam was made to rest on the corbels and a 20 mm thick neoprene pad was used to cushion the assembly. Grouting was then done using the locally available material SikaGrout 214, which is a non-shrink modified cementitious grout with shrinkage compensation in both plastic and hardened states. For the case of PC-B specimen, steel plates were used instead of the neoprene pad. Other than that, the assembly procedure was the same. In the PC-B specimen, apart from the corbel rebar being grouted with beam, a welded connection was also used. This was accomplished by having an angle section 200 × 75 × 10 mm embedded in the beam and the corbel before casting as shown in Fig. 7(h). A steel plate 150 × 370 × 20 mm was used to rest the beams on the corbel surfaces. After grouting was done using the same SikaGrout 214, the two angles and the steel plate were welded along the edge using a line weld.

2.3 Material Properties

Ready-mix concrete was used for casting the test specimens. The specified concrete strength measured as per the ASTM C39/C39M (ASTM, 2010) at the time of the test was 35 MPa. For steel rebars, tensile tests were conducted according to ASTM E8/E8M (ASTM, 2009) and the average values of yield strength of ϕ8 and ϕ16 mm rebars were 525 and 526 MPa, respectively.

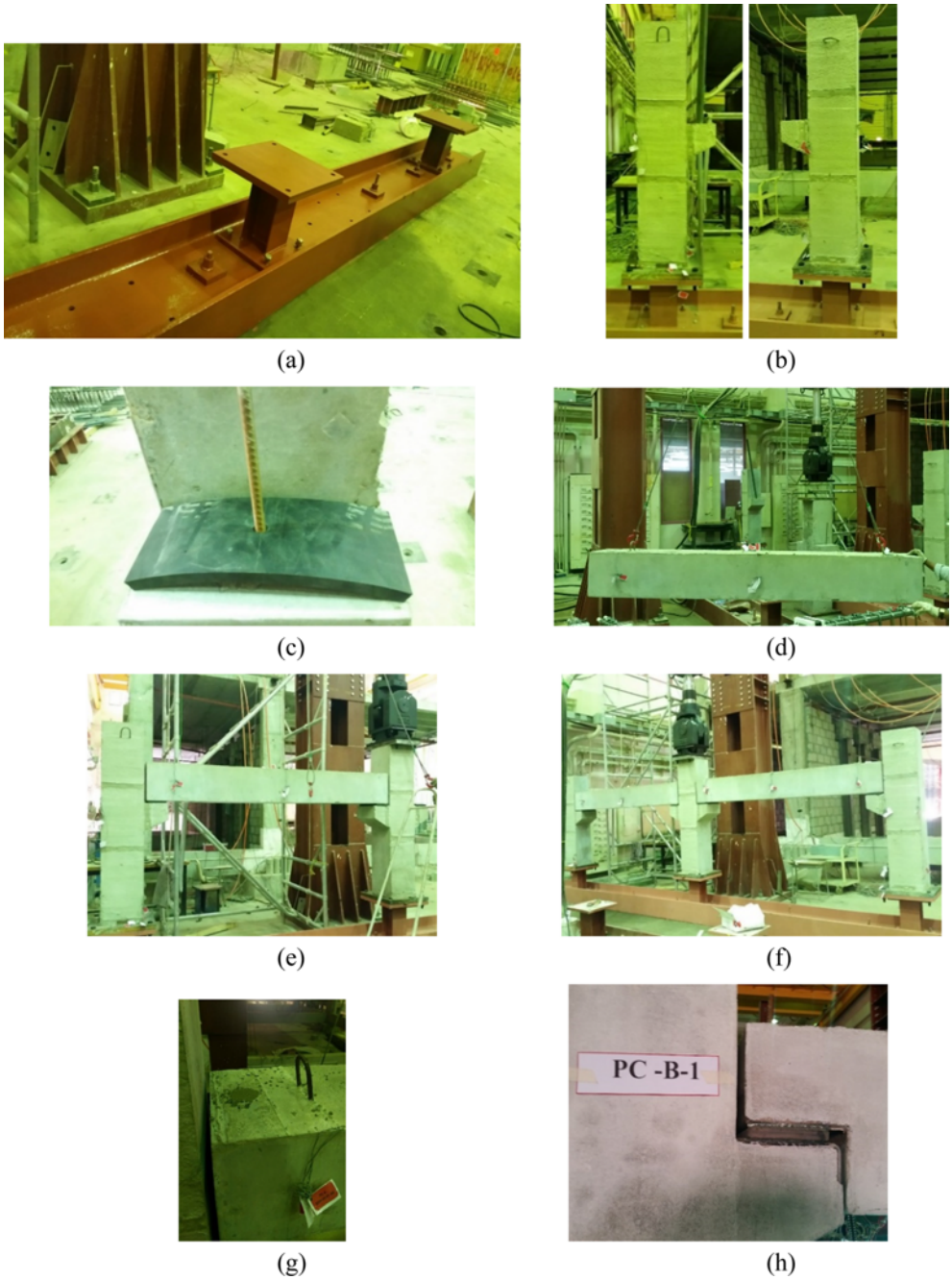

Fig. 7. Assembly of Precast Specimens on Test Rig: (a) Steel Rail for Supporting Test Specimen, (b) Columns Erected on Steel Rail, (c) Neoprene Pad Placed on Column Corbel Before Beam Resting, (d) Beams Being Carried by Overhead Crane for Erection, (e) Beam Erection Completed using Overhead Crane, (f) Specimen Assembly Completed with all Members Erected, (g) PC-A Specimen Beam Pocket Filled with Grouting Material, (h) PC-B Specimen with Line Welding Along Edge of Embedded Angle

However, the average values of tensile strength of ϕ8 and ϕ16 mm rebars were 550 and 651 MPa, respectively.

2.4 Test Setup and Procedure

A steel loading frame shown in Fig. 8(a), which exists in the structural lab of King Saud University was used for testing the specimens. The susceptibility of a building to blast loading may cause a sudden column removal, which may end up with partial or total progressive collapse of the building. This was represented by removing the support of the test column and exerting a dynamic load on that column using an actuator of 1000 kN capacity. The test specimen was placed in position on steel rails that were fixed to the strong floor of the lab. The test column was then strongly attached to the actuator using four high strength threaded rods of 25-mm diameter. Bases of the exterior columns were affixed to the steel rails.

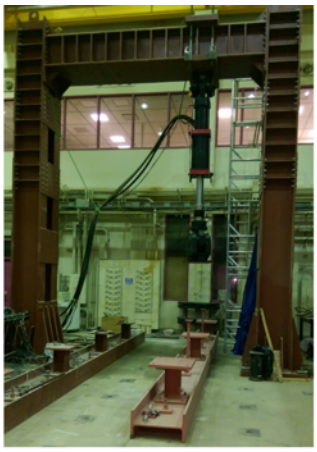

(a)

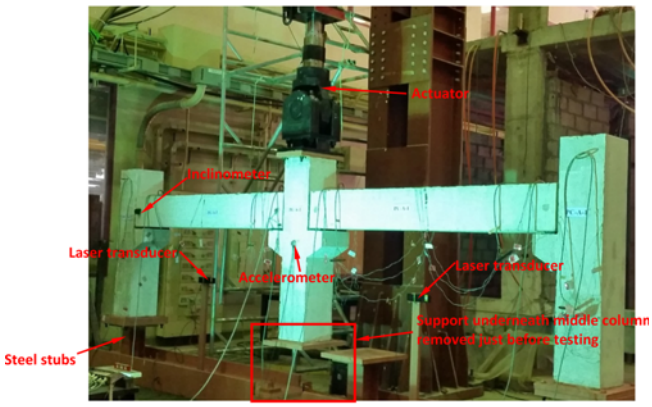

(b)

Fig. 8. Test Setup and Instrumentation Layout: (a) Loading Frame with Actuator and Rails for Supporting Specimen, (b) Instrumented Specimen PC-A (Taken from Elsanadedy *et al.* (2017)).

A high speed data acquisition system was utilized to collect data at speed of 1 k/s. The individual beam and column members of the specimens were instrumented for measuring strains in the longitudinal and transverse rebars using strain gages. The center column and beam mid-span displacements were measured using extremely precise laser transducers. The instrumentation program also included measurement of end rotations of the beams using dual-axis inclinometers. The three-dimensional vibration of the specimen was recorded using a tri-axial accelerometer. Fig. 8(b) depicts the complete instrumentation layout for the precast specimen PC-A.

After strongly connecting the actuator with the test column, its support was removed. All sensors were set to zero reading at this stage. Since the ultimate load capacity of the specimen is not known prior to testing and in order to mimic the post-peak softening behavior of the test frame, a displacement controlled loading was adopted for the middle column. The typical target displacement-time history used for specimen testing is given in Fig. 9. A 1000-kN servo-controlled fatigue-rated MTS actuator was employed for load application. In real progressive collapse scenarios due to blast threats, the column is removed suddenly with very high speed, which cannot be accommodated in the

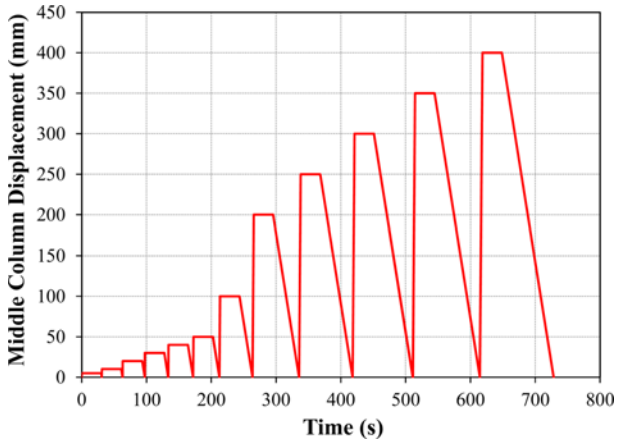

Fig. 9. Typical Target Displacement-time History for Specimen Testing

experiments due to the limits of the used actuator. The rate of loading used in this study was 100 mm/s, which is low compared with the actual scenarios. The loading rate adopted (i.e. 100 mm/s) was the maximum possible for the actuator and thus the inertial effects in experiments were of smaller scale than expected in a column-removal scenario. It is worth mentioning here that the increase in stresses due to the inertial forces is partly compensated by the enhanced material strength due to strain rate effect and thus the error introduced because of the reduced inertial effects is relatively small. The load on the test column was applied using the actuator in cycles of incremental vertical displacement in each cycle with sufficient rest period after each state of loading (Fig. 9). The increments were used to capture the behavior of specimen at different displacement levels. The rest period was utilized for taking note of the observations and marking the cracks. The unloading was done at a slow speed of 5 mm/s. Data recording during the test was done and the results for all specimens were analyzed to study the collapse mechanism of the entire frame specimen as well as individual frame members.

3. Test Results and Discussion

Table 2 shows a summary of the behavior of test specimens in terms of: (i) peak load without self-weight, (ii) middle column displacement at peak load, (iii) beam mid-span deflection at peak load, (iv) load at yielding of beam bottom rebars, (v) middle column displacement at yielding of beam bottom rebars, (vi) middle column displacement at ultimate state, (vii) energy ductility at ultimate state, and (viii) displacement ductility. It should be noted that the ultimate state used in Table 2 is defined as the state where the load drops to 80% of its peak value based on New Zealand Standard-1992 (Standards New Zealand 1992). It should be also noted that the energy ductility index (m_E) shown in Table 2 is estimated as per Emadi and Hashemi (2011) from

$$\mu_E = \frac{1}{2}\left(\frac{E_u}{E_y} + 1\right) \tag{1}$$

where E_u is the energy of the frame specimen at ultimate state

Table 2. Comparison of Load-displacement Characteristics for Test Specimens*

Specimen ID	P_y (kN)	P_u (kN)	$\Delta_{u,c}$ (mm)	$\Delta_{u,b}$ (mm)	Δ_y (mm)	Δ_u (mm)	E_y (kN.m)	E_u (kN.m)	μ_Δ	μ_E
PC-A	No steel yielding	12.8	145	66	No steel yielding	265	No steel yielding	2.5	-	-
PC-B	No steel yielding	23.4	250	116	No steel yielding	284	No steel yielding	5.5	-	-
MC-SMF	145	228	144	65	25.6	269	2.1	54.5	10.5	13.3

*P_y = load at yielding of bottom beam rebars; P_u = peak load; $\Delta_{u,c}$ = middle column displacement at peak load; $\Delta_{u,b}$ = beam mid-span deflection at peak load; Δ_y = middle column displacement at yielding of bottom beam rebars; Δ_u = middle column displacement at ultimate state; E_y = energy dissipated at first yield of beam bottom rebars; E_u = energy dissipated at ultimate state; μ_Δ = displacement ductility = Δ_u/Δ_y; μ_E = energy ductility.

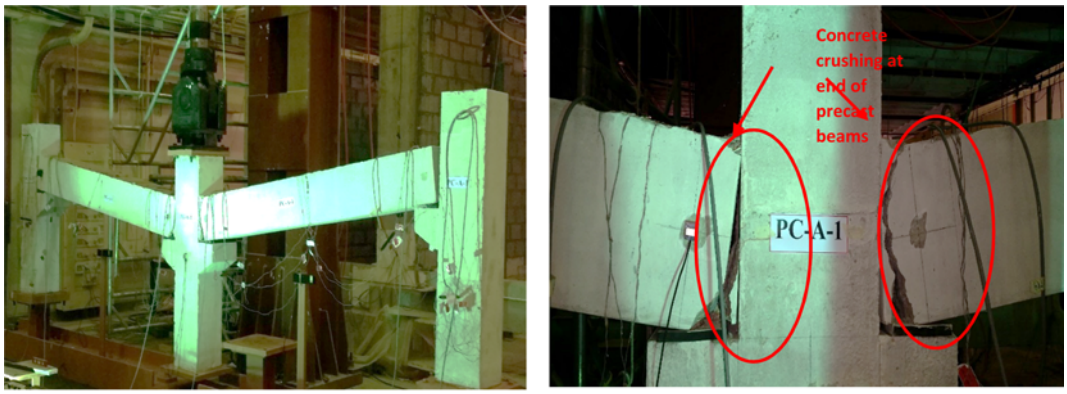

Fig. 10. Final Deformed Shape for PC-A Specimen at a Middle Column Displacement of 350 mm: (a) Final Deformed Shape, (b) Failure of Middle Joint

(area under load-displacement curve up to ultimate displacement) and E_y is the energy of the frame specimen at first yield of beam bottom rebars (area under load-displacement curve up to yield displacement). In the following sections, the test results have been presented in terms of mode of failure, load-displacement behavior and the results of the strain gages.

3.1 Modes of Failure

Final modes of failure for the three specimens at interior and exterior joints are illustrated in Figs. 10 to 12.

3.1.1 PC-A Specimen

As seen in Fig. 10(a) for specimen PC-A, a proper hinge behavior was observed in the specimen which was expected. During the test, both the beams of specimen PC-A were found to rotate at their ends until the interior ends came in contact with the middle column, and the ultimate mode of failure was due to concrete crushing at the location of interior beam-column joint as seen in Fig. 10(b). Other than this, no other damage was observed in any members of specimen PC-A including beams and columns. It should be also noted that at the exterior connection end, the neoprene pad underneath the beam helped to absorb the energy thereby protecting the exterior corbel from damaging.

3.1.2 PC-B Specimen

Figure 11 presents the final failure mode for the PC-B frame at the interior beam-column connection. As seen from the figure, a proper hinge behavior was noticed and the left and right beams were found to rotate at their ends until failure occurred due to debonding of steel angles of the corbels near the interior column. Some minor cracks were also formed in the corbels of the middle column. As a result of beam rotation, stress concentration was observed in the column corbels at locations where the beam was bearing on the corbel. This resulted in bearing stresses thereby causing diagonal splitting cracks in column corbels as shown in Fig. 11(c). Debonding of some part of the steel angle from corbel concrete was also noticed. There was no noticeable damage to both the beams as well as the exterior columns.

3.1.3 MC-SMF Specimen

Figure 12 depicts the final failure mode for the MC-SMF frame at the middle beam-column joint. Failure of specimen MC-SMF occurred around the middle column due to plastic hinge formation in the beam area near the connection zone. As seen in Fig. 12(b), a plastic hinge was formed near the middle joint due to large plastic strains in the bottom steel rebars of the beam beyond their yield state (indicated by wide flexural cracks) accompanied with concrete crushing in the compression zone. As seen from the figure, failure of beam was not exactly symmetric on both sides of the middle column. In this case flexural action developed until the formation of plastic hinges at the middle joint. At this point, there was rapid yielding of the bottom beam reinforcement of the middle joint. Thereafter, yielding of the top beam rebars at the outer joints indicated the formation of the plastic hinge and that the full flexural capacity was reached. Flexural cracks were also observed in both the end columns,

(a)

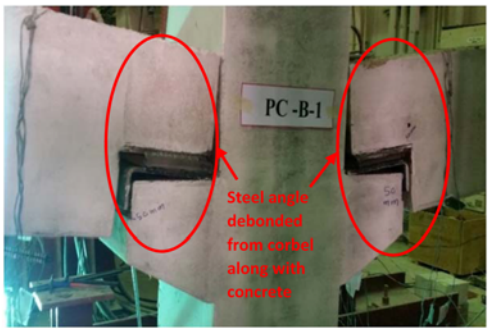

(b)

(c)

Fig. 11. Final Deformed Shape for PC-B Specimen at a Middle Column Displacement of 400 mm: (a) Final Deformed Shape, (b) Failure of Middle Joint, (c) Failure at End Joint

(a)

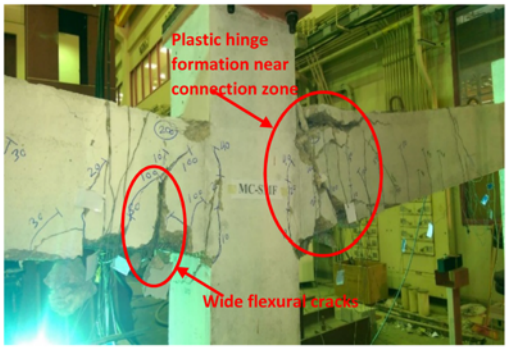

(b)

(c)

Fig. 12. Final Deformed Shape for MC-SMF Specimen at a Middle Column Displacement of 400 mm: (a) Final Deformed Shape, (b) Failure of Middle Joint, (c) Failure at End Joint

whereas the columns were also found to have rotated at joint locations as a result of the large deformation of the middle column (Fig. 12(c)). This rotation of the columns indicated that the beam ends were not effectively restrained. Owing to this rotation, along with the limitation of actuator stroke and the discontinuity of beam members beyond the end columns, there was no development of the catenary action. As a result there was no further increase in load-carrying capacity of the frame. Catenary action is usually developed at a displacement of more than one-beam depth and it fully utilizes the reserve tensile strength of steel reinforcement. Since the displacement was limited to close to the beam depth there was no possibility of developing catenary action in this frame.

3.2 Load-displacement Characteristics

Displacement-time histories for middle column and the mid-span of the beam are shown in Fig. 13 for the three test specimens. As seen from the graph, for all target displacement levels, beam mid-span displacement of specimens PC-A and PC-B is about 46% of the middle column displacement thereby indicating expected hinge behavior of the frame. This behavior is confirmed from the theoretical beam-deformation mechanism depicted in Fig. 14(a), from which it can be inferred that the theoretical beam mid-span displacement equals 48% of the center column displacement. However, for monolithic specimen MC-SMF, beam mid-span displacement was about 55% of the middle column displacement up to a target displacement level of 50 mm

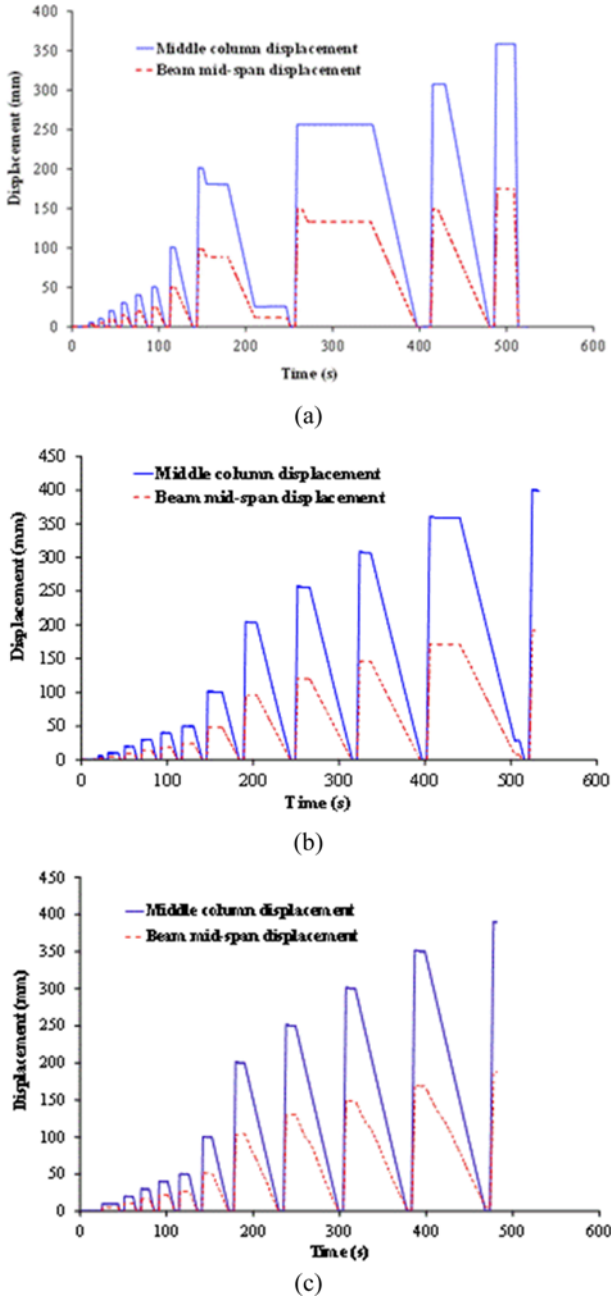

Fig. 13. Displacement-time History for: (a) Specimen PC-A, (b) Specimen PC-B, (c) Specimen MC-SMF

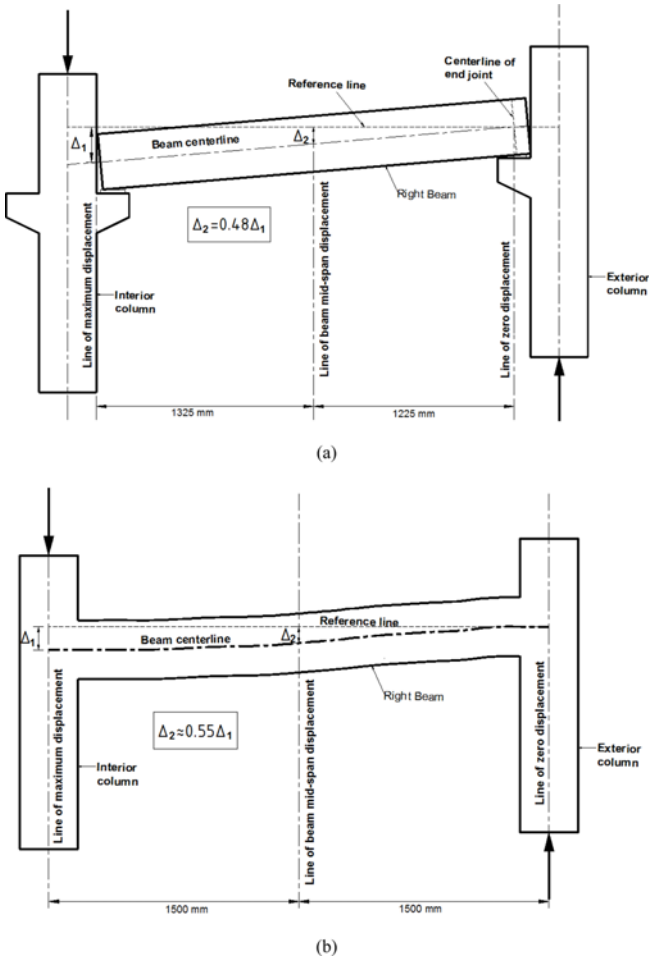

Fig. 14. Theoretical Beam-deformation Mechanism for: (a) Precast Specimen PC-A (or PC-B), (b) Monolithic Specimen MC-SMF

at the center column location, which indicates an elastic curve anticipated in continuous beams. This behavior is supported from the theoretical beam-deformation mechanism sketched in Fig. 14(b) for monolithic specimen with small middle column displacement. Yet, for middle column displacement levels more than 50 mm, the plastic hinge started to form at both beam ends and the beam turned into a hinge mechanism similar to that shown in Fig. 14(a), thus having a mid-span displacement of about 45% of the middle column displacement.

Load versus middle column displacement hysteresis and envelopes are presented as shown in Fig. 15 for all test specimens. The curves shown in Fig. 15 do not include the self-weight of the specimen. Comparison of load-displacement envelopes for test frames is shown in Fig. 16. Fig. 15(a) reveals that precast concrete buildings with connection type A is very vulnerable to progressive collapse once the supporting column is lost in an extreme event. The peak load (not including self-weight of frame specimen PC-A) was 12.8 kN. It was obtained in the 8th loading cycle corresponding to a target displacement of 200 mm. It is clear from Figs. 15 and 16 that the precast connection type B is better than connection type A in terms of its resistance to progressive collapse when subjected to sudden removal of column as a result of unexpected loading scenarios. For the precast specimen PC-B, the peak load (not including self-weight of the frame) was 23.5 kN. It was obtained in the 10th loading cycle corresponding to a target displacement of 300 mm as shown in Fig. 15(b).

For monolithic specimen MC-SMF, as seen in Figs. 15(c) and 16, the load-displacement envelope can be divided into four stages. The AB segment can be considered as the elastic stage, during which the relationship between the load and the vertical displacement of middle column is linear, without obvious

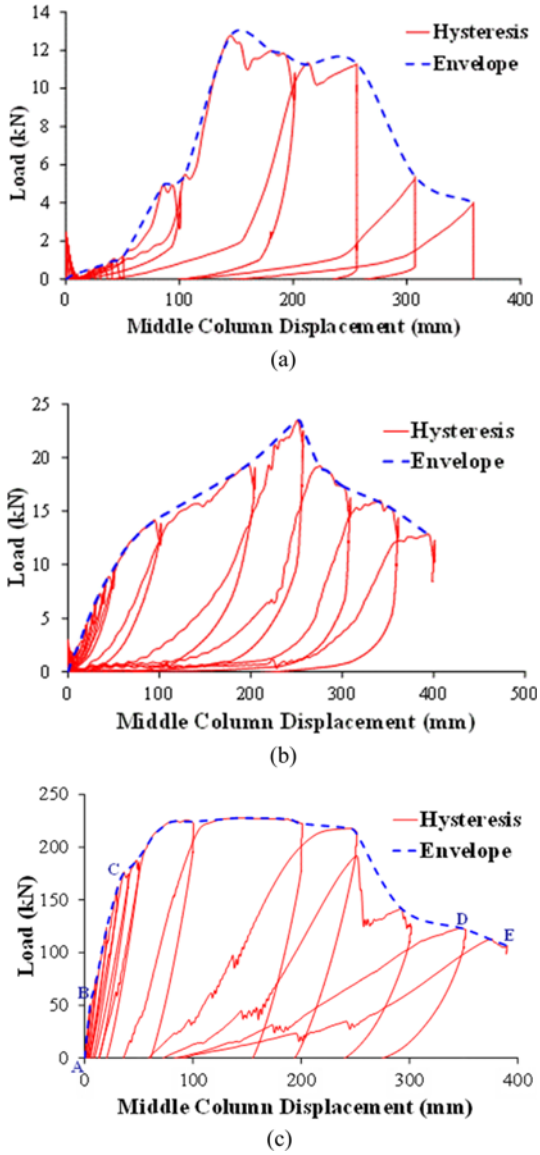

Fig. 15. Load-displacement Hysteresis for: (a) Specimen PC-A, (b) Specimen PC-B, (c) Specimen MC-SMF

destruction in the frame specimen. The BC segment is the start of the inelastic stage. The load is in a nonlinear relationship with the increase of displacement and the secant stiffness begins to drop at this stage. From the recorded steel strains, it was noticed that the longitudinal rebars at the ends of beams started to yield, indicating the formation of plastic hinges in the beams. And, most of the steel rebars at the ends of beams had yielded at Point C. The CD segment is the plastic hinge stage. Plastic hinges at the ends of beams were formed and the frame gradually turned into a plastic stress system. Concrete crushing was observed from Point C and concrete spalling appeared at a later period in this stage. The progressive collapse resistance of the specimen began to decrease after reaching a middle column displacement of about 250 mm as shown in Fig. 15(c). The DE segment is the catenary action stage. The flexural capacity of beams was almost

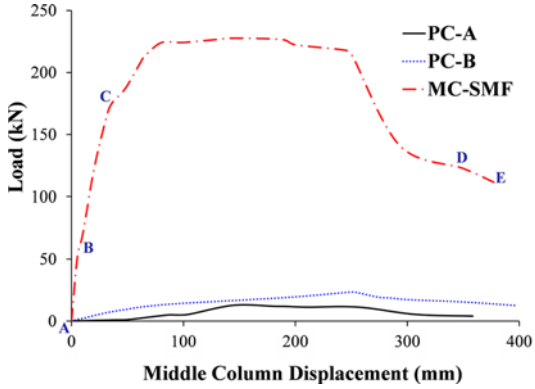

Fig. 16. Load-displacement Envelope Comparison for Test Specimens

lost at this stage. At the inner beam-column connection, the flexural tension cracks extended through the compression zones, demonstrating the formation of the catenary mechanism at the inner joint. However, because the outer beam-column joints were unable to provide enough anchorage for the longitudinal steel bars in the beams, the bearing capacity of the frame at the catenary action stage decreased continuously with the increment of the vertical displacement. The structure entered an irreversible collapse process and the test was terminated due to limitation of the actuator stroke (at Point E). From the load-displacement comparison presented in Fig. 16, it is clear that the monolithic specimen MC-SMF (with continuous top and bottom beam rebars) has excellent performance compared with the two precast specimens PC-A and PC-B. The peak load (not including self-weight) resisted by specimen MC-SMF was 228 kN which is about 17.8 and 9.7 times of that for specimens PC-A and PC-B, respectively. This peak load was obtained in the 8th loading cycle corresponding to a target displacement of 200 mm as shown in Fig. 15(c). In addition, and as depicted from Table 2, displacement and energy ductility ratios of specimen MC-SMF were very high. The excellent performance of the monolithic specimen MC-SMF was expected due to the continuity of the beam rebars and hence the redundancies in the load paths. As seen from Table 2 and the load-displacement curves, the displacement energy is almost negligible for both precast specimens PC-A and PC-B thereby indicating no ductility at all in the system, which shows their high vulnerability to progressive collapse.

3.3 Strain Gage Results

Summary of strain gage results of longitudinal rebars of beams, columns and corbels is depicted in Table 3 for the three test specimens at the peak load level. For specimen PC-A, due to the discontinuity of beam reinforcement at the connection zone, a minor strain of 74 me (close to zero) was recorded in the beam bottom rebars at peak load and hence the specimen has no displacement ductility to dissipate the energy exerted in the system upon sudden column removal as seen in Tables 2 and 3. For specimen PC-B, as shown in Table 3, a small strain of 622 me was measured in the beam bottom rebars at peak load.

Table 3. Comparison of Steel Strains at Peak Load for Test Specimens*

Specimen ID	Longitudinal rebars of beam				Longitudinal rebars of exterior column		Corbel top longitudinal rebars
	At face of interior column		At face of exterior column		Inner rebars	Outer rebars	
	Bottom rebars	Top rebars	Bottom rebars	Top rebars			
PC-A	74 με	–60 με	–30 με	60 με	-42 με	50 με	247 με
PC-B	622 με	–170 με	–140 με	475 με	–80 με	153 με	556 με
MC-SMF	95189 με	–4100 με	–1700 με	14957 με	–2500 με	16912 με	–

*Positive sign means tensile strain and negative sign means compressive strain.

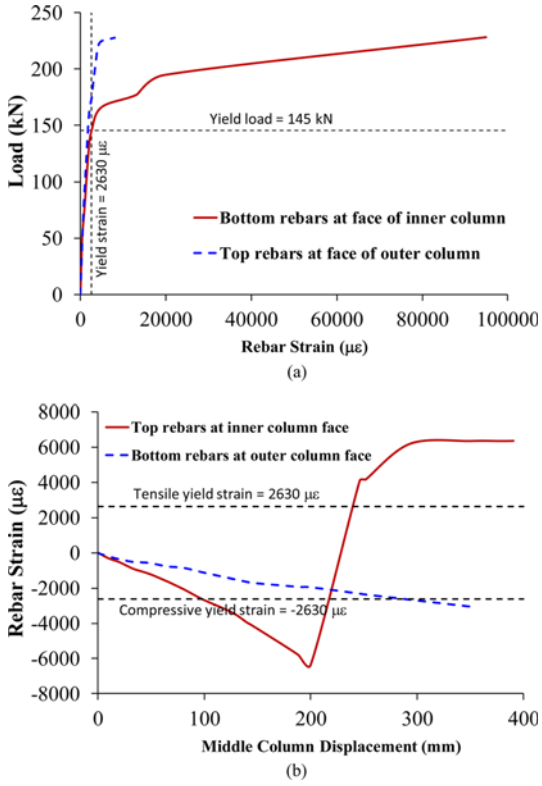

Fig. 17. Strain Gage Results for Longitudinal Beam Rebars of Specimen MC-SMF: (a) Longitudinal Tension Rebars, (b) Longitudinal Compression Rebars

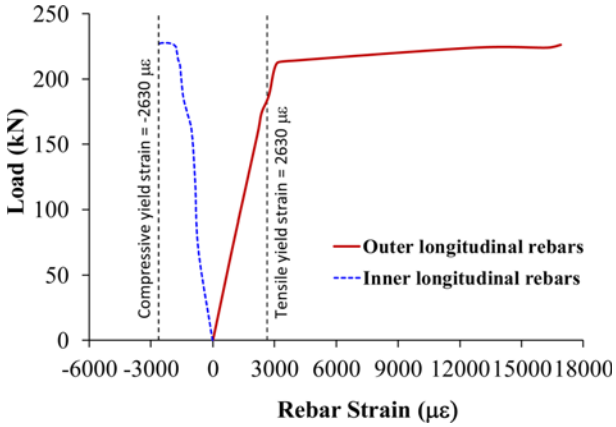

Fig. 18. Strain Gage Results foR Longitudinal Column Rebars of Specimen MC-SMF

Therefore, the specimen has no displacement ductility to dissipate the input energy in the system upon sudden column removal, which makes it vulnerable to progressive collapse. For monolithic specimen MC-SMF, at peak load, a tensile strain of 95189 me (about 36 times the yield strain) was recorded in the bottom rebars of the beam (Table 3). From the table, it is indicated that for specimen MC-SMF, all the tension steel rebars at the ends of beams had yielded and large tensile strains were recorded at the peak load level thereby indicating plastic hinge formation at the ends of beams as previously discussed.

Strain gage results for beam steel rebars of specimen MC-SMF are presented in Figs. 17(a) and 17(b) for tension and compression bars, respectively. As expected both the top (outer column face) and bottom (inner column face) rebars were in tension and were found to have exceeded the yield strength. As seen in Fig. 17(b), both the top (inner column face) and bottom (outer column face) steel rebars of the beam were in compression until a displacement of 200 mm, after which the top rebars at the middle joint went from compression to tension and then yielded in tension. This indicated that until 200 mm of displacement, the flexural cracks had still not reached the top rebars whereas as the displacement increased above 200 mm, the flexural cracks penetrated the beam depth and reached the top rebars thereby applying tensile stresses on the top rebars at inner column face.

Figure 18 shows load versus steel strain of longitudinal rebars of outer columns. Strains in both inner and outer column rebars are depicted in the figure. As seen from the figure, the outer longitudinal rebars are in tension and have yielded whereas, the inner column rebars are in compression and have also yielded. This indicates flexural bending of the outer columns.

From Fig. 17(b), it is clear that all beam rebars were not in tension, which prevented the full formation of catenary action. This can be attributed to the limitation of the actuator stroke, which in turn limited the middle column displacement to 400 mm and also indicates the insufficient restraint provided by the outer columns. The beam-column joints could not provide enough anchorage for longitudinal steel rebars at the beam ends, which directly affected the development of the catenary forces. The research results of Yi *et al.* (2008) and Yu and Tan (2013) showed that the bearing capacities of the catenary action stage generally exceed that of flexural capacity of frame beam. In another study, Wang *et al.* (2016) observed that the damage of beam-column joints limits the development of the catenary action when the joints are damaged before the frame beam. Thus,

beam-column joints should be further enhanced in progressive collapse-resistant design to gain a better progressive collapse resistance. In addition, the ductility and load-carrying capacity of the tested monolithic frame in the current study could have been further improved if catenary action had developed. Other studies by Kang and Tan (2015) and Kang *et al.* (2015) also indicated the development of catenary action at high displacements of middle columns in precast beam-column assemblages. However, in their studies the precast beams and columns were joined together by cast-in-place topping using regular concrete as well as engineered cementitious composites.

4. Conclusions

This paper presents the outcomes of an experimental program to study the progressive collapse resistance of RC precast beam-column assemblages in comparison with a monolithic frame. Results have been discussed in terms of failure modes, load-displacement curves and strain gage findings. The major conclusions derived from this study can be summarized as follows:

1. Precast connection type B is relatively better than connection type A in terms of its resistance to progressive collapse. The progressive collapse resistance capacity of precast specimen PC-B was about 1.8 times of that for specimen PC-A. However, the two types of precast connections (A and B) were found to have a very high potential of progressive collapse due to negligible ductility and lack of continuity in beam-column joints and hence absence of redundancies in the collapse load paths.
2. The monolithic specimen MC-SMF with continuous top and bottom beam reinforcement had significantly higher collapse load compared to other two specimens, as progressive collapse resistance capacity of monolithic specimen was 17.8 and 9.7 of that for precast specimens PC-A and PC-B, respectively. The displacement and energy ductility ratios of specimen MC-SMF were very large.
3. The monolithic specimen MC-SMF was found to exhibit structural mechanism of flexural action. Failure was due to the formation of plastic hinges at beam ends. However, the development of catenary action was inhibited due to: limitation of actuator stroke, discontinuity of beams beyond the exterior columns and the insufficient restraint provided by outer columns.
4. The high potential for progressive collapse found in two types of prevalent beam-column connections investigated in this study highlights the need for the rehabilitation of beam-column connections in existing precast buildings. Moreover, it is recommended to search for innovative beam-column connections for providing collapse load path redundancy in the event of sudden column-loss scenario in new designs of precast RC frames.

Acknowledgements

This work is based on the Project funded by the National Plan for Science, Technology and Innovation (MAARIFAH), King Abdulaziz City for Science and Technology, Kingdom of Saudi Arabia, Award Number (12-BUI2620-02).

References

ACI Committee 318 (2008). *Building code requirements for structural concrete and commentary*, ACI 318-08, American Concrete Institute, Detroit, MI, USA.

Al-Salloum, Y. A., Almusallam, T. H., Khawaji, M. Y., Ngo, T., Elsanadedy, H. M., and Abbas, H. (2015). "Progressive collapse analysis of RC buildings against internal blast." *Advances in Structural Engineering,* Vol. 18, No. 12, pp. 2181-2192, DOI: 10.1260/1369-4332.18.12.2181.

Allen, D. E. and Schriever, W. R. (1972). "Progressive collapse, abnormal load, and building codes, structural failure: Modes, causes, responsibilities." *Proceedings of the American Society of Civil Engineers,* New York, USA.

Almusallam, T. H., Elsanadedy, H. M., Abbas, H., Alsayed, S. H., and Al-Salloum, Y. A. (2010). "Progressive collapse analysis of a RC building subjected to blast loads." *Structural Engineering and Mechanics – An International Journal,* Vol. 36, No. 3, pp. 301-319, DOI: 10.12989/sem.2010.36.3.301.

ASTM (2009). *Standard test methods for tension testing of metallic materials (ASTM E8/E8M),* American Society for Testing and Materials, West Conshohocken, PA, USA.

ASTM (2010). *Standard test method for compressive strength of cylindrical concrete specimens (ASTM C39/C39M)*, American Society for Testing and Materials, West Conshohocken, PA, USA.

Bao, Y., Kunnath, S. K., El-Tawil, S., and Lew, H. S. (2008). "Macromodel-based simulation of progressive collapse: RC frame structures." *Journal of Structural Engineering –ASCE,* Vol. 134, No. 7, pp. 1079-1091, DOI: 10.1061/(ASCE)0733-9445(2008)134:7(1079).

Choi, H. K., Choi, Y. C., and Choi, C. S. (2013). "Development and testing of precast concrete beam-to-column connections." *Engineering Structures,* Vol. 56, pp. 1820-1835, DOI: 10.1016/j.engstruct.2013.07.021.

Choi, J. and Chang, D. (2009). "Prevention of progressive collapse for building structures to member disappearance by accidental actions." *Journal of Loss Prevention in the Process Industries,* Vol. 22, pp. 1016-1019, DOI: 10.1016/j.jlp.2009.08.020.

Dat, P. X., Haiand, T. K., and Jun, Y. (2015). "A simplified approach to assess progressive collapse resistance of reinforced concrete framed structures." *Engineering Structures,* Vol. 101, pp. 45-57, DOI: 10.1016/j.engstruct.2015.06.051.

Elkoly, S. and El-Ariss, B. (2014). "Progressive collapse evaluation of externally mitigated reinforced concrete beams." *Engineering Failure Analysis,* Vol. 40, pp. 33-47, DOI: 10.1016/j.engfailanal.2014.02.002.

Elsanadedy, H. M., Almusallam, T. H., Al-Salloum, Y. A., and Abbas, H. (2017). "Investigation of precast RC beam-column assemblies under column-loss scenario." *Construction and Building Materials*, Vol. 142, pp. 552-571, DOI: 10.1016/j.conbuildmat.2017.03.120.

Elsanadedy, H. M., Almusallam, T. H., Alharbi, Y. R., Al-Salloum, Y. A., and Abbas, H. (2014). "Progressive collapse potential of a typical steel building due to blast attacks." *Journal of Constructional Steel Research,* Vol. 101, pp. 143-157, DOI: 10.1016/j.jcsr.2014.05.005.

Emadi, J. and Hashemi, S. H. (2011). "Flexural study of high strength RC beams strengthened with CFRP plates." *World Academy of Science, Engineering and Technology,* Vol. 78, pp. 380-384.

Ertas, O., Ozden, S., and Ozturan, T. (2006). "Ductile connections in

precast concrete moment resisting frames." *PCI Journal,* Vol. 5, pp. 2-12, DOI: 10.15554/pcij.05012006.66.76.

Joshi, M. K., Murty, C. V., and Jaisingh, M. P. (2005). "Cyclic behaviour of precast RC connections." *Indian Concrete Journal,* Vol. 79, pp. 43-50.

Kang, S. B. and Tan, K. H. (2015). "Behaviour of precast concrete beam-column sub-assemblages subject to column removal." *Engineering Structures,* Vol. 93, pp. 85-96, DOI: 10.1016/j.engstruct.2015.03.027.

Kang, S. B., Tan, K. H., and Yang, E. (2015). "Progressive collapse resistance of precast beam-column sub-assemblages with engineered cementitious composites." *Engineering Structures,* Vol. 98, pp. 186-200, DOI: 10.1016/j.engstruct.2015.04.034.

Livermore Software Technology Corporation (LSTC). (2007). *LS-DYNA user's keyword manual (nonlinear dynamic analysis of structures in three dimensions) Volume 1*, Version 971, LSTC, Livermore, California, USA.

Panedpojaman, P., Jina, P., and Limkatanyu, S. (2016). "Moment capacity and fire protection of the welded plate joint for precast members." *Archives of Civil and Mechanical Engineering,* Vol. 16, pp. 753-766, DOI: 10.1016/j.acme.2016.04.017.

Parastesh, H., Hajirasouliha, I., and Ramezani, R. (2014). "A new ductile moment-resisting connection for precast concrete frames in seismic regions: An experimental investigation." *Engineering Structures,* Vol. 70, pp. 144-157, DOI: 10.1016/j.engstruct.2014.04.001.

Peakau, O. A. and Cui, Y. (2006). "Progressive collapse simulation of precast panel shear walls during earthquakes." *Computers & Structures,* Vol. 84, pp. 400-412, DOI: 10.1016/j.compstruc.2005.09.027.

Pourasil, M. B., Mohammadi, Y., and Gholizad, A. (2017). "A proposed procedure for progressive collapse analysis of common steel building structures to blast loading." *KSCE Journal of Civil Engineering*, Vol. 21, No. 6, pp. 2186-2194, DOI: 10.1007/s12205-017-0559-0.

Sasani, M., Bazan, M., and Sagiroglu, S. (2007). "Experimental and analytical progressive collapse evaluation of actual reinforced concrete structure." *ACI Structural Journal,* Vol. 104, No. 6, pp. 731-39.

Shariatmadar, H. and Beydokhti, E. Z. (2011). "Experimental investigation of precast concrete beam to column connections subjected to reversed cyclic loads." In: *Proceedings of the 6th International Conference on Seismology and Earth Engineering*. Tehran, Iran, pp. 1-9.

Standards New Zealand. (1992). *Code of practice for general structural design and design loadings for buildings 1 (NZS 4203: 1992)*, New Zealand Standard.

Vidjeapriya, R. and Jaya, K. P. (2012). "Behaviour of precast beam-column mechanical connections under cyclic loading." *Asian Journal of Civil Engineering (Building and Housing),* Vol. 13, pp. 233-245.

Vidjeapriya, R. and Jaya, K. P. (2013). "Experimental study on two simple mechanical precast beam column connections under reverse cyclic loading." *Journal of Performance of Constructed Facilities,* Vol. 27, pp. 402-414, DOI: 10.1061/(ASCE)CF.1943-5509.0000324.

Wahjudi, D.I., Suprobo, P., and Sugihardjoa, H. (2014). "Behavior of precast concrete beam-to-column connection with U and L-bent bar anchorages placed outside the column panel - experimental study." *2nd Int Conf on Sustainable Civil Engineering Structures and Construction Materials (SCESCM 2014)*. Procedia Engineering 95, pp. 122-131.

Yi, W., He, Q., Xiao, Y., and Kunnath, S. (2008). "Experimental study on progressive collapse-resistant behavior of reinforced concrete frame structures." *ACI Structural Journal,* Vol. 105, No. 4, pp. 433-439.

Yu, J. and Tan, K. (2013). "Experimental and numerical investigation on progressive collapse resistance of reinforced concrete beam column sub-assemblages." *Engineering Structures,* Vol. 55, pp. 90-106, DOI: 10.1016/j.engstruct.2011.08.040.